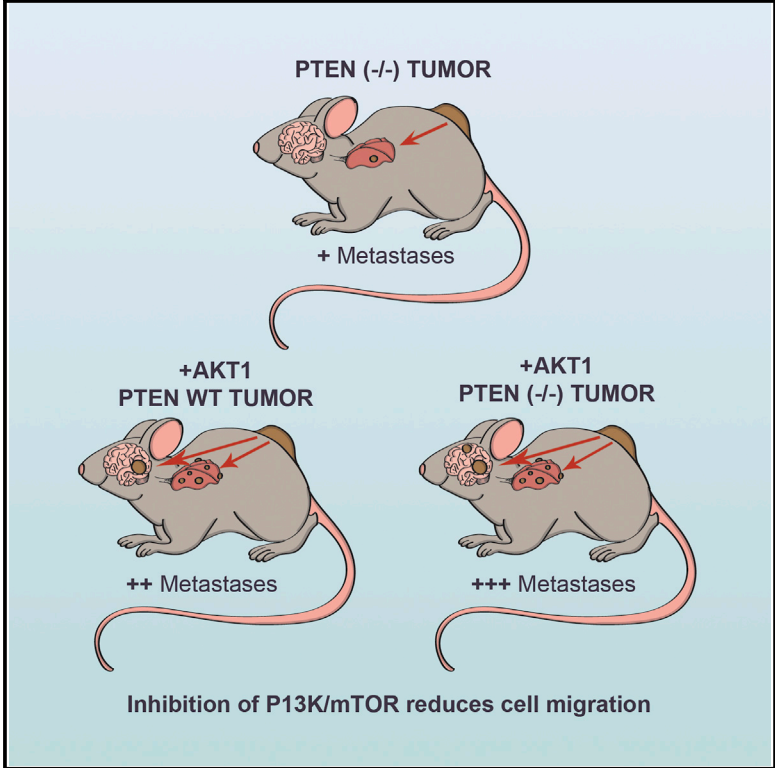# AKT1 Activation Promotes Development of Melanoma Metastases

Graphical Abstract

Authors

Joseph H. Cho, James P. Robinson, Rowan A. Arave, ..., Matthew W. VanBrocklin, Martin McMahon, Sheri L. Holmen

Correspondence

sheri.holmen@hci.utah.edu

In Brief

AKT signaling has been implicated in melanoma metastasis; however, the ability of activated AKT1 to promote melanoma metastasis in vivo has not been explored. Cho et al. show that expression of activated AKT1 in $BRAF^{V600E}/Cdkn2a^{Null}$ melanomas is sufficient to promote tumor cell dissemination to the lungs and brain.

Highlights

- Expression of activated AKT1 promotes melanoma formation and metastasis

- Loss of *Pten* cooperates with AKT1 activation to promote melanoma metastasis

- mTOR signaling downstream of AKT1 is implicated in driving metastasis

CellPress

AKT1 Activation Promotes Development of Melanoma Metastases

Joseph H. Cho,[1,9] James P. Robinson,[2,9] Rowan A. Arave,[3] William J. Burnett,[1] David A. Kircher,[1] Guo Chen,[4] Michael A. Davies,[4] Allie H. Grossmann,[5] Matthew W. VanBrocklin,[1,6,7] Martin McMahon,[1,7,8] and Sheri L. Holmen[1,6,7,*]

[1]Department of Oncological Sciences, University of Utah Health Sciences Center, Salt Lake City, UT 84112, USA
[2]Hormel Institute, University of Minnesota, Austin, MN 55912, USA
[3]Department of Chemistry, University of Utah Health Sciences Center, Salt Lake City, UT 84112, USA
[4]Department of Melanoma Medical Oncology, University of Texas MD Anderson Cancer Center, Houston, TX 77030, USA
[5]Department of Pathology, University of Utah Health Sciences Center, Salt Lake City, UT 84112, USA
[6]Department of Surgery, University of Utah Health Sciences Center, Salt Lake City, UT 84112, USA
[7]Huntsman Cancer Institute, University of Utah Health Sciences Center, Salt Lake City, UT 84112, USA
[8]Department of Dermatology, University of Utah Health Sciences Center, Salt Lake City, UT 84112, USA
[9]Co-first author
*Correspondence: sheri.holmen@hci.utah.edu
http://dx.doi.org/10.1016/j.celrep.2015.09.057

SUMMARY

Metastases are the major cause of melanoma-related mortality. Previous studies implicating aberrant AKT signaling in human melanoma metastases led us to evaluate the effect of activated AKT1 expression in non-metastatic BRAF^{V600E}/Cdkn2a^{Null} mouse melanomas in vivo. Expression of activated AKT1 resulted in highly metastatic melanomas with lung and brain metastases in 67% and 17% of our mice, respectively. Silencing of PTEN in BRAF^{V600E}/Cdkn2a^{Null} melanomas cooperated with activated AKT1, resulting in decreased tumor latency and the development of lung and brain metastases in nearly 80% of tumor-bearing mice. These data demonstrate that AKT1 activation is sufficient to elicit lung and brain metastases in this context and reveal that activation of AKT1 is distinct from PTEN silencing in metastatic melanoma progression. These findings advance our knowledge of the mechanisms driving melanoma metastasis and may provide valuable insights for clinical management of this disease.

INTRODUCTION

Recent approvals of more efficacious therapies have significantly shifted the treatment paradigm for melanoma and have provided much needed breakthroughs in this disease (Girotti et al., 2014). Despite these recent therapeutic advances, the majority of melanoma deaths continue to be due to metastasis, which demands further investigation into the molecular mechanisms driving distant dissemination of this disease.

Members of the phosphatidylinositol 3-kinase (PI3K)/AKT pathway have been implicated in melanoma initiation, progression, invasion, and metastasis. Activation of AKT in this disease occurs most commonly through silencing of the tumor suppressor PTEN (reviewed in Madhunapantula and Robertson, 2011). PTEN is a phosphatase with activity against both lipid and protein substrates (Chalhoub and Baker, 2009). Its major substrate is phosphatidylinositol-3,4,5-triphosphate (PIP$_3$), which recruits AKT to the membrane, where it is activated by phosphorylation. PTEN specifically dephosphorylates the 3′ position of PIP$_3$ to create phosphatidylinositol-4,5-bisphosphate (PIP$_2$) and thereby suppresses membrane recruitment and downstream signaling of AKT. Loss of PTEN results in increased levels of PIP3 and subsequent AKT activation.

We have previously demonstrated that PTEN silencing combined with expression of BRAF^{V600E} in mouse melanocytes in vivo results in melanoma formation (Dankort et al., 2009). Our current study builds on these findings and demonstrates that ectopic expression of activated AKT1 strongly potentiates metastasis in the context of mutant BRAF^{V600E} and silencing of INK4A and ARF. Additionally, PTEN silencing cooperates with active AKT1 to accelerate both tumor formation and metastasis. This model provides a valuable tool to further define the mechanisms that promote melanoma metastases and a powerful platform to advance the development of anti-melanoma therapies.

RESULTS

BRAF^{V600E}/Cdkn2a^{Null} Melanomas Are Not Metastatic

To evaluate melanoma metastasis in the context of specific genetic alterations, we utilized an established melanoma mouse model based on the RCAS/TVA system that allows for targeted delivery of specific genes to post-natal melanocytes (VanBrocklin et al., 2010). This system utilizes a viral vector, RCASBP(A), hereafter referred to as RCAS, and its receptor, TVA. Transgenic mice that express TVA under the control of the dopachrome tautomerase (DCT) promoter allow targeting of the virus, and expression of the genes it contains, specifically to melanocytes. To assess metastasis using this model in the context of mutationally activated BRAF^{V600E}, we compound generated *Dct::TVA;BRaf^{CA};Cdkn2a$^{lox/lox}$* mice (VanBrocklin et al., 2010) carrying a conditional Cre-activated allele of *Braf*.
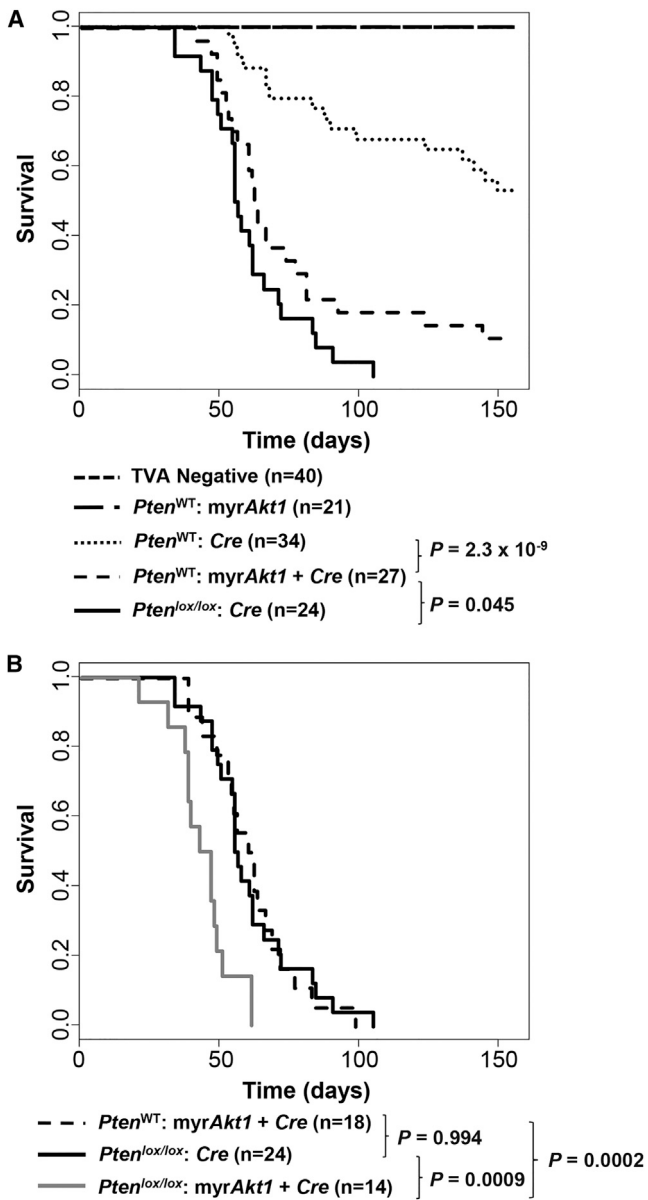
CrossMark

Figure 1. Kaplan-Meier Percent Survival Curves for BRAF-Induced Tumors

(A) Loss of *Pten* or expression of myrAKT1 significantly increases tumor incidence and reduces tumor latency. *Dct::TVA;Braf*^{CA}*;Cdkn2a*$^{lox/lox}$ mice (*Pten*^{WT}) were injected at birth with viruses containing either *Cre* (small dashed line, n = 34) or myr*Akt1* and *Cre* (wide dashed line, n = 27) as indicated. *Dct::TVA;Braf*^{CA}; *Cdkn2a*$^{lox/lox}$*;Pten*$^{lox/lox}$ mice (*Pten*$^{lox/lox}$) were injected with viruses encoding *Cre* (solid black line, n = 24). TVA-negative *Braf*^{CA}*;Cdkn2a*$^{lox/lox}$ and *Braf*^{CA}; *Cdkn2a*$^{lox/lox}$*;Pten*$^{lox/lox}$ mice injected with *Cre*-containing viruses (narrow dashed line, n = 40) and *Pten*^{WT} mice injected with myr*Akt1*-containing viruses (off-width dashed line, n = 21) yielded no tumors and are shown as negative controls. A significant difference was observed between the survival of *Pten*^{WT} mice injected with *Cre*-containing viruses and *Pten*^{WT} mice injected with myr*Akt1*- and *Cre*-containing viruses (p = 2.3 × 10^{-9}). A significant difference was also observed between the survival of *Pten*^{WT} mice injected with *Cre*- and myr*Akt1*-containing viruses and *Pten*$^{lox/lox}$ mice injected with *Cre*-containing viruses (p = 0.045).

(B) Loss of *Pten* cooperates with AKT1 activation to accelerate tumor formation. Comparison of the mice whose tumors were found to express myrAKT1

The *Braf*^{CA} allele expresses wild-type BRAF prior to Cre-mediated recombination after which BRAF^{V600E} is expressed from the normal chromosomal locus (Dankort et al., 2007). The *Cdkn2a*^{lox} allele expresses normal INK4A and ARF prior to Cre-mediated recombination after which expression of both p16^{INK4A} and p19^{ARF} is extinguished (Aguirre et al., 2003).

Newborn *Dct::TVA;Braf*^{CA}*;Cdkn2a*$^{lox/lox}$ mice were injected subcutaneously with an RCAS virus encoding *Cre* to induce BRAF^{V600E} expression with concomitant silencing of INK4A and ARF in melanocytes. While *Braf*^{CA}*;Cdkn2a*$^{lox/lox}$ mice lacking Dct::TVA injected with RCAS:*Cre* remained tumor free for the duration of the study (150 days, n = 40), 47% (16/34) of the *Dct::TVA;Braf*^{CA}*;Cdkn2a*$^{lox/lox}$ mice infected with the RCAS:*Cre* virus developed tumors at the site of injection (Table S1). The mean survival for tumor-bearing mice in this cohort was 88.9 ± 8.6 days (Figure 1A). All major organs were examined at euthanasia, but no melanoma metastases were observed in any of the tumor-bearing mice.

PTEN Silencing Increases Tumor Incidence and Reduces Tumor Latency but Does Not Significantly Enhance Metastasis to Distant Organs

Because BRAF^{V600E} cooperates with PTEN silencing to induce metastatic melanoma (Dankort et al., 2009), we generated *Dct::TVA;Braf*^{CA}*;Cdkn2a*$^{lox/lox}$*;Pten*$^{lox/lox}$ (*Pten*$^{lox/lox}$) mice. The *Pten*^{lox} allele used here expresses normal PTEN prior to Cre-mediated recombination after which deletion of the exon 5 sequence generates a *Pten* null allele (Zheng et al., 2008). Newborn *Dct::TVA;Braf*^{CA}*;Cdkn2a*$^{lox/lox}$*;Pten*$^{lox/lox}$ mice were injected subcutaneously with RCAS:*Cre* to induce BRAF^{V600E} with concomitant silencing of INK4A, ARF, and PTEN in melanocytes. Importantly, control mice, *Braf*^{CA}*;Cdkn2a*$^{lox/lox}$*;Pten*$^{lox/lox}$ lacking *Dct::TVA* infected with RCAS:*Cre* remained tumor free for the duration of the study (150 days, n = 40). Tumors developed at the site of injection in all of the *Dct::TVA*-positive *Braf*^{CA}; *Cdkn2a*$^{lox/lox}$*;Pten*$^{lox/lox}$ mice infected with RCAS:*Cre* viruses (n = 24). The mean survival was 57.8 ± 3.4 days in this cohort (Figure 1A; Table S1). Expression of Cre was assessed by RT-PCR (Figure S1A), and recombination of *Pten*^{lox} was confirmed by PCR in all of the tumors that developed (Figure S1B). In these mice, lung metastases were detected in 8.3% (2/24) of the mice whose melanomas had PTEN silencing. However, using a Fisher's exact test, we determined that this difference was not statistically significant when compared with mice whose tumors expressed PTEN (p = 0.5).

Expression of Activated AKT1 Promotes Melanoma Formation and Distant Metastasis

Several studies have shown that PTEN silencing confers a different phenotype than AKT activation (Majumder et al., 2003; Wang et al., 2003). Therefore, we evaluated the effect of

(wide dashed line, n = 18) and mice whose tumors lacked *Pten* revealed no significant difference (p = 0.994) (solid black line, n = 24). However, the survival of *Pten*$^{lox/lox}$ mice injected with myr*Akt1*- and *Cre*-containing viruses (solid gray line, n = 14) differed significantly from the survival of *Pten*$^{lox/lox}$ mice injected with *Cre*-containing viruses (p = 0.0009) and *Pten*^{WT} mice injected with myr-*Akt1*- and *Cre*-containing viruses (p = 0.0002).

mutationally activated AKT1 on melanoma formation and progression in vivo. Newborn *Dct::TVA;Braf^CA;Cdkn2a^lox/lox* (*Pten*^WT) mice were injected subcutaneously with RCAS viruses encoding myristoylated (myr) *Akt1* alone or in combination with viruses encoding *Cre*. Virally delivered myrAkt1 contains a hemagglutinin (HA) epitope tag to discern expression from endogenous AKT1. While *Dct::TVA;Braf^CA;Cdkn2a^lox/lox* mice injected with viruses encoding myr*Akt1* alone remained tumor free for the duration of the study (150 days, n = 21), 88% (24/27) of the mice injected with both myr*Akt1*- and *Cre*-encoding viruses developed tumors at the site of injection (Figure 1A; Table S1). The mean survival of the tumor-bearing mice in this cohort was 65.3 ± 4.7 days (Figure 1A). It is important to note that AKT1 expression is not required for tumor formation in the context of BRAF^V600E/INK4A-ARF silencing; tumors develop in nearly half of *Dct::TVA;Braf ^CA;Cdkn2a^lox/lox* mice infected with viruses encoding *Cre* only (Figure 1A). Of the 24 mice that developed tumors when injected with myr*Akt1* and *Cre* viruses, AKT1 expression was detected in 18 of the tumors by IHC for the HA epitope tag on myrAKT1 (Figure S2). The mean survival was 58.9 ± 3.5 in this myrAKT1-confirmed cohort (Figure 1B; Table S1). A significant difference in survival was observed between mice whose tumors expressed myrAKT1 and those without myrAKT1 (p = 2.3 × 10^{-9}). A significant difference in survival was also observed between the *Pten^lox/lox* cohort injected with viruses encoding *Cre* only when compared with all of the mice in the *Pten*^WT cohort injected with two separate viruses encoding *Cre* and myr*Akt1* (p = 0.045) (Figure 1A; Table S1). However, comparison between the mice whose tumors were found to express myrAKT1 by immunohistochemistry (IHC) (18/24) and mice whose tumors lacked PTEN revealed no significant difference in survival (p = 0.994; Figure 1B). All major organs were examined in tumor-bearing mice. Interestingly, lung metastases were observed in 67% (12/18) and brain metastases were observed in 17% (3/18) of the mice whose tumors expressed myrAKT1. This difference was statistically significant when compared with both the *Pten*^WT and the *Pten^lox/lox* cohorts injected with RCAS:*Cre* viruses (p < 0.0001).

PTEN Silencing Cooperates with Activated AKT1 to Accelerate Melanomagenesis and to Promote Distant Metastasis

Our data revealed differences in the development of distant metastases between cohorts of mice whose tumors lacked PTEN compared with mice whose tumors expressed myrAKT1. Therefore, we assessed whether PTEN silencing could cooperate with myrAKT1 activation to promote melanoma formation and progression. To test this, newborn *Dct::TVA; Braf^CA;Cdkn2a^lox/lox; Pten^lox/lox* mice were injected subcutaneously with viruses encoding myr*Akt1* and *Cre*. Tumors developed at the site of injection in all of the mice in this cohort (n = 14), and myrAKT1 expression was detected in all of these tumors by anti-HA IHC (Figure S3). Expression of Cre was assessed by RT-PCR (Figure S1C), and recombination of *Pten* was confirmed by PCR in all of the tumors that developed (Figure S1D). Interestingly, melanomas with concomitant PTEN silencing and myrAKT1 expression had significantly reduced survival compared with mice whose tumors only had PTEN silencing (p = 0.0009) or ex-

pressed myrAKT1 in the presence of PTEN (p = 0.0002). The mean survival in this cohort was 42.1 ± 2.8 days (Figure 1B; Table S1). All major organs were examined, and lung and brain metastases were observed in 71% (10/14) and 79% (11/14) of the mice, respectively. A comparison of the sites of metastases revealed no significant difference in lung metastases (p = 1.0), but there was a statistically significant difference in brain metastases between tumors driven by myrAKT1 in the presence or absence of PTEN (p = 0.0009).

Histological Characterization of the Mouse Melanomas Reveals Features Similar to the Human Disease

Melanomas arising in *Dct::TVA;Braf^CA;Cdkn2a^lox/lox* mice infected with both RCAS:*Cre* and RCAS:myr*Akt1* encoding viruses consisted primarily of short spindle cells, occasional epithelioid cells, and with high-grade nuclear features, including prominent nucleoli. Intratumoral hemorrhage, coagulative tumor necrosis, and non-brisk inflammation (tumor infiltrating lymphocytes) were variably noted (Figure 2A). Mitotic figures were abundant and the majority of the cells expressed the Ki67 proliferation marker (Figure 2B). The activity of BRAF^V600E was assessed by IHC for pERK as a surrogate (Figure 2C). The melanocytic origin of these tumors was established by their immunoreactivity for a pan-melanoma cocktail consisting of antibodies to HMB-45, a pre-melanosomal glycoprotein gp100, and melanoma antigen recognized by T cells-1 (MART-1) (Figure 2D). The combination of positivity for both HMB-45 and MART-1 is highly supportive of a melanoma diagnosis (Ohsie et al., 2008). Upon gross examination, lesions were visible on the surface of the lungs (Figure 2E) and microscopic examination confirmed the morphologic features of malignancy (Figures 2F and 2G). AKT1 expression was detected in the metastases by IHC for the HA epitope tag on myrAKT1 (Figure 2H). Brain metastases were also observed in *Dct::TVA;Braf ^CA;Cdkn2a^lox/lox* mice infected with both *Cre* and myr*Akt1* containing viruses (Figure 2I). Expression of myrAKT1 was confirmed in the brain metastases by IHC for the HA tag on virally delivered myrAKT1 (Figure 2J).

Primary tumors from each of the cohorts described above were assessed for the presence of phosphorylated AKT (pS473) by IHC and compared with BRAF^V600E/INK4A-ARF^Null melanomas (Figures 3A and 3B). As expected, active pS473-AKT was detected in tumors lacking PTEN, expressing myrAKT1, or both (Figures 3C–3H). The levels of pS473-AKT were also assessed by immunoblot analysis of lysates generated from fragments of tumors with wild-type PTEN, lacking PTEN, expressing myrAKT1, or lacking PTEN and expressing myrAKT1 (Figure 4A). In agreement with the IHC data, PTEN^Null melanomas displayed higher levels of pS473-AKT (Figure 4B). Expression of myrAKT1 was confirmed by immunoblotting for the HA epitope tag on myrAKT1 (Figure 4A) and quantified (Figure 4B). Cre-mediated expression of mutationally activated BRAF was assessed using an antibody specific for BRAF^V600E. Activity of the MAPK pathway was assessed by analysis of phosphorylated ERK expression. Total levels of ERK were similar between the samples. As expected, the levels of total AKT were higher in the melanomas engineered to express myrAKT1 and a wider band representing the larger molecular mass of myrAKT1 was detected on the total AKT blot (Figure 4A).
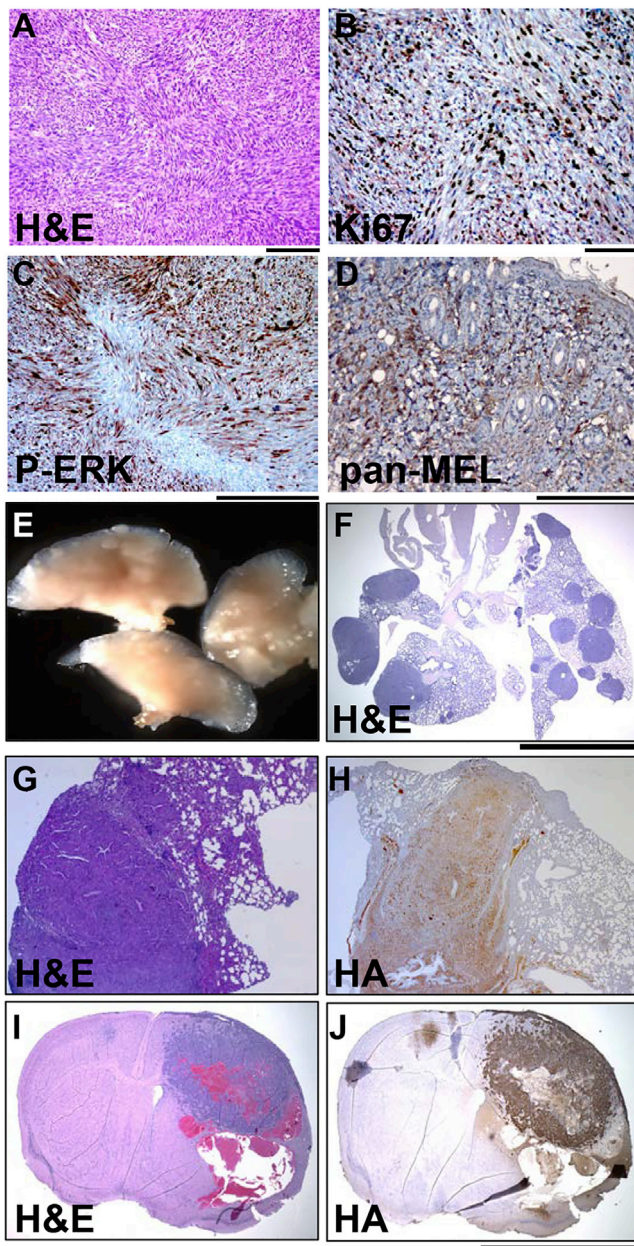
Figure 2. Histological Analysis of BRAF^V600E and myrAKT1-Induced Tumors

(A–D) Tumors were induced in *Dct::TVA;Braf^CA;Cdkn2a^lox/lox* mice (*Pten*^WT) by subcutaneous injection of newborn mice with viruses containing myr*Akt1* and *Cre*. (A_ Representative tumor H&E. (B) Ki67 IHC. (C) P-ERK IHC. (D) IHC for HMB-45, gp100, and MART-1 (pan-MEL). Scale bars represent 200 μm.

(E–H) Metastases to the lung were observed in *Pten*^WT mice injected with myr*Akt1*- and *Cre*-containing viruses. (E) Representative gross lung with multiple metastatic lesions. (F) Low-magnification H&E of a lung with multiple melanoma metastases. (G) Higher-magnification H&E of a lung metastasis. (H) HA IHC confirmed expression of myrAKT1. Scale bar represents 6 mm.

(I and J) Brain metastases were observed in *Pten*^WT mice injected with myr*Akt1*- and *Cre*-containing viruses. (I) H&E of representative melanoma brain metastasis. (J) HA IHC confirmed expression of myrAKT1. Scale bar represents 5 mm.
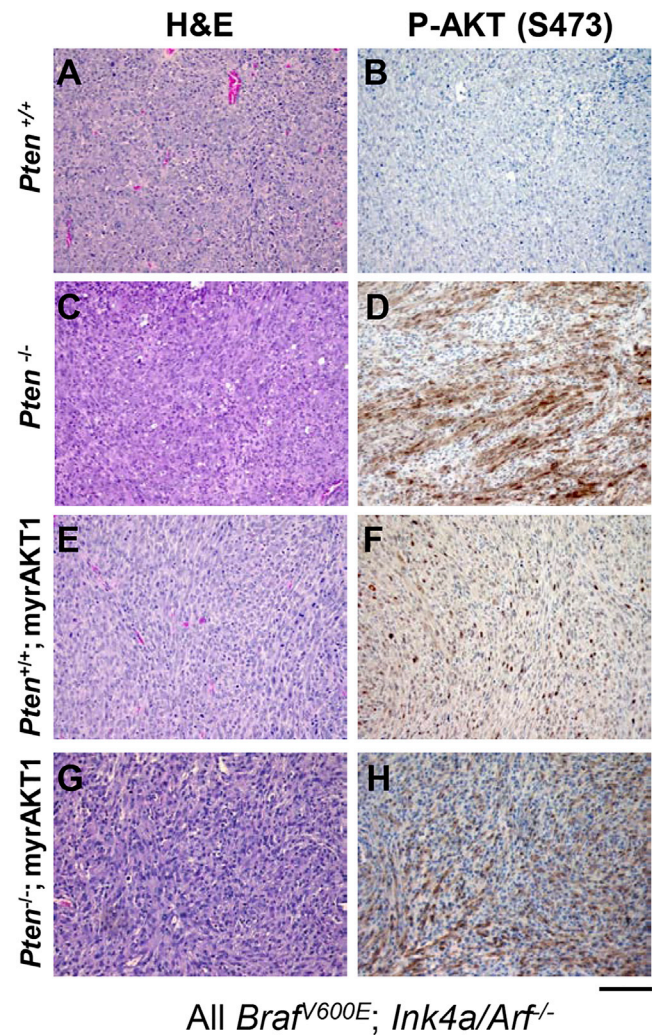

All *Braf^V600E; Ink4a/Arf^-/-*

Figure 3. Comparison of AKT Activity in Mutant BRAF Melanomas

The left panel (A, C, E, and G) shows a representative H&E of the primary tumor, and the right panel (B, D, F, and H) shows phosphorylated AKT (p-AKT) (pS473) IHC staining of an adjacent section. All tumors lack *Cdkn2a* expression and express mutant BRAF. *Pten* status and myrAKT1 expression are indicated on the left. Pertinent tumor genotypes are as follows: (A and B) BRAF^V600E;*Cdkn2a*^−/−; (C and D) BRAF^V600E;*Cdkn2a*^−/−;*Pten*^−/−; (E and F) BRAF^V600E ;*Cdkn2a*^−/−; myrAKT1; and (G and H) BRAF^V600E ;*Cdkn2a*^−/−;*Pten*^−/−;myrAKT1. Scale bar represents 200 μm.

Reverse-Phase Protein Array Analysis Reveals Increased mTOR Signaling in Tumors Expressing myrAKT1

To define differences in signaling between the melanomas lacking PTEN and those expressing myrAKT1 in a high-throughput manner we used a reverse-phase protein array (RPPA) approach. RPPA allows quantitative analysis of protein levels and activation using small amounts of protein (Liotta et al., 2003). Tumor-enriched protein isolates from five PTEN^Null and four myrAKT1-expressing melanomas were analyzed by RPPA. The heatmap in Figure 5 shows the results of unsupervised hierarchical clustering of the results of this analysis, which showed a
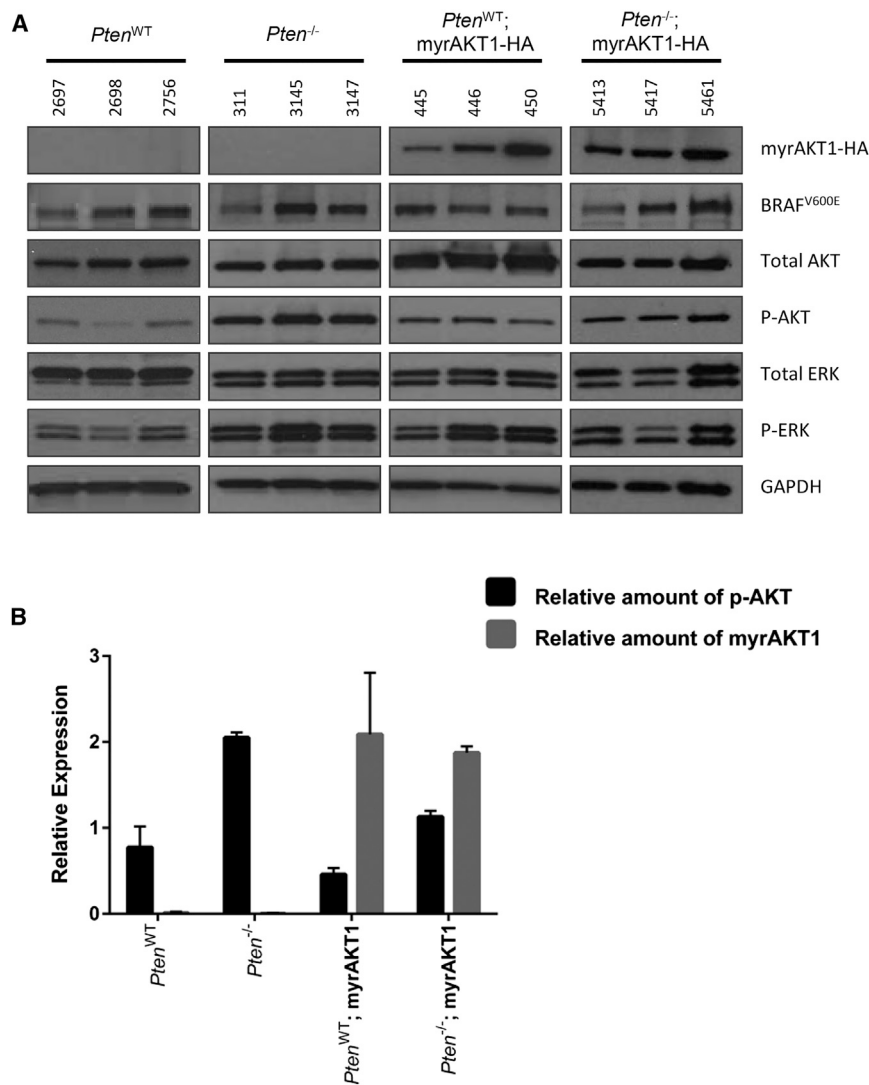
A

(A) Expression of myrAKT1-HA was assessed in 12 different tumor samples from four different genotypes: $Cdkn2a^{-/-}$;BRAF^{V600E} (2,697, 2,698, 2,756), $Cdkn2a^{-/-}$;BRAF^{V600E};$Pten^{-/-}$ (311, 3,145, 3,147), $Cdkn2a^{-/-}$;BRAF^{V600E};myrAKT1 (445, 446, 450), and $Cdkn2a^{-/-}$;BRAF^{V600E};$Pten^{-/-}$;myrAKT1 (5,413, 5,417, 5,461). The cells were lysed in SDS lysis buffer and separated on 4%–20% gradient polyacrylamide gels. Virally delivered myr$Akt1$ expression was detected with an antibody to the HA epitope tag on myrAKT1. Activation of AKT was evaluated by blotting for p-AKT and comparing the levels of total AKT expression. Mutant BRAF expression was confirmed and downstream activity was evaluated by blotting for phosphorylated ERK1/2 (p-ERK1/2) and comparing the levels of total ERK1/2 expression. GAPDH expression was used as a loading control.

(B) Bar graphs illustrate the relative quantification of p-AKT (black bars) and myrAKT1 expression (gray bars) from the four different tumor genotypes. Relative levels of p-AKT were calculated by densitometry and normalized to total AKT levels. The levels of myrAKT1 were determined by calculating the densitometry for HA and normalizing to GAPDH levels. Data are presented as mean ± SEM.

mTOR signaling, we treated normal human embryonic melanocytes (NHEM) and human melanoma cell lines A375, M14-MEL, and CACL, which harbor mutant BRAF, with DMSO or the pharmacological inhibitor NVP-BEZ-235 (BEZ-235), a dual PI3K/mTOR inhibitor. While very little migration was observed for NHEM, all three melanoma cell lines were highly migratory in this assay. Treatment with BEZ-235 (2 μmol/l) significantly reduced migration in the NHEM and all three melanoma cell lines over a 48-hr time period compared with DMSO treatment alone (Figure S5A). To examine the effects of BEZ-235 on signal pathway activity, extracts of melanoma cells treated with BEZ-235 (2 μmol/l) for 24 hr were subjected to immunoblot analysis (Figure S5B). BEZ-235 elicited a 96% reduction in phosphorylated AKT (pAKT; pS473) in A375 and M14 melanoma cells and a 90% reduction in phosphorylated AKT in CACL cells, which displayed the highest levels of pAKT among the three cell lines.

DISCUSSION

Through combined PTEN silencing and mutational activation of AKT1 in the context of the BRAF^{V600E} oncoprotein kinase and INK4A-ARF silencing, we have established an autochthonous model of spontaneous lung and brain metastases that is similar to the human disease. Furthermore, we provide compelling evidence that AKT1 activation plays a critical role in promoting melanoma metastasis to distant organs in vivo
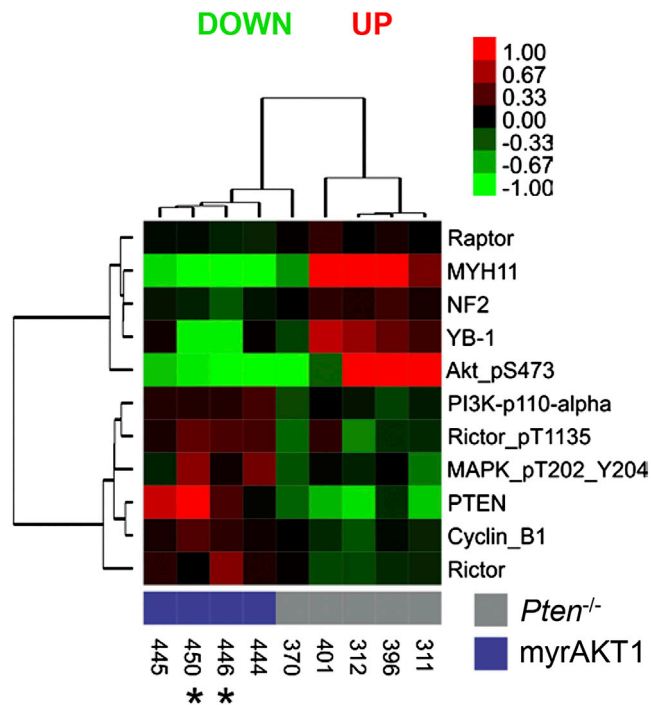
significant difference in protein modification/expression levels (n = 11; p < 0.05 by unpaired t testing) between the five PTEN^{Null} tumor samples and the four myrAKT1-expressing melanoma samples. A list of all 131 epitopes assessed with their respective p values is presented in Table S2. As expected, lower levels of PTEN expression were detected in the melanoma samples from $Pten^{lox/lox}$ mice. In agreement with both the IHC and immunoblot analyses, a higher level of pS473-AKT was observed in the PTEN^{Null} tumor samples. Interestingly, components of the mammalian target of rapamycin (mTOR) signaling pathway (e.g., RAPTOR, RICTOR, NF2, and MYH11) were significantly different between the two groups (Figure 5; Figure S4).

Pharmacological Inhibition of PI3K and mTOR Reduces Melanoma Cell Migration

Pharmacological inhibition of PI3K and mTOR has been shown to inhibit melanoma cell growth both in vitro and in vivo and interfere with angiogenesis (reviewed in Sznol et al., 2013). To determine the dependence of melanoma cell migration on PI3K/

Figure 5. RPPA Analysis of Protein from *Pten* Null and myrAKT1 Melanomas

Protein was isolated from *Cdkn2a*$^{-/-}$;BRAF^{V600E};*Pten*$^{-/-}$ (*Pten*$^{-/-}$) and *Cdkn2a*$^{-/-}$;BRAF^{V600E};myrAKT1 (myrAKT1) tumors; expression was assessed by RPPA. Log2 expression data were subjected to unsupervised clustering, and the results are presented as a heatmap. Tumors were labeled *Pten*$^{-/-}$ (gray squares) or myrAKT1 (blue squares). The heatmap shown represents the proteins and phosphorylated proteins with a significant difference (p < 0.05 using unpaired t tests) between myrAKT1 and *Pten*$^{-/-}$ tumors. An asterisk (*) denotes a primary tumor from a mouse with brain metastasis.

via a mechanism that is independent of, yet augmented by, PTEN silencing.

We observed dramatically increased distant metastasis in mice bearing tumors driven by activated AKT1 compared with *Pten* loss. Moreover, AKT1 activation cooperated with *Pten* loss to accelerate tumor formation and further increase dissemination to the lungs and brain. Our data suggest that aberrant AKT1 signaling in melanoma extends beyond the modulation of PIP3 levels by PTEN and PI3K. Our previous work demonstrated that the growth of BRAF^{V600E}/PIK3CA^{H1047R} melanomas depends on AKT signaling, but this dependency was not observed for the growth of BRAF^{V600E}/PTEN^{Null} melanomas (Marsh Durban et al., 2013). Our current study builds on these findings and demonstrates that BRAF^{V600E}/PTEN^{Null}/INK4A-ARF^{Null} melanomas are not significantly metastatic (<10%) compared to controls, while ectopic expression of myrAKT1 strongly potentiates metastasis in BRAF^{V600E}/INK4A-ARF^{Null} melanomas. These data suggest that there are likely to be PI3'-lipid signaling thresholds in melanoma cells that can confer different properties on the melanoma cell as demonstrated recently (Deuker et al., 2015).

Interestingly, PTEN deficient melanomas had significantly higher levels of phosphorylated AKT (Figures 3D, 4A, and 5)

compared with tumors expressing myrAKT1 (Figures 3F, 3H, 4A, and 5) yet significantly fewer distant metastases. In mammals there are three isoforms of AKT, namely AKT1, AKT2 and AKT3. While the AKT isoforms share ∼80% amino acid sequence identity, in vivo studies demonstrate that they have both redundant and non-overlapping functions (Gonzalez and McGraw, 2009). Compound AKT isoform knockout mice demonstrate that AKT1 exhibits functional redundancy with AKT2 and AKT3, but the reverse relationships lack full reciprocation (Dummler et al., 2006; Peng et al., 2003; Yang et al., 2005). Thus, for our studies of in vivo AKT signaling in melanoma, expression of activated AKT1 facilitates signaling in the broadest context. There have been conflicting reports regarding which isoforms of AKT are phosphorylated following PTEN loss in melanoma cells (Nogueira et al., 2010; Stahl et al., 2004). It is possible that signaling from AKT1 differs from the signaling that results from the activation of AKT isoforms with PTEN silencing. Some studies suggest that AKT isoforms have opposing functions with regards to tumorigenesis (Linnerth-Petrik et al., 2014; Maroulakou et al., 2007). It is possible that specific isoforms of AKT differentially contribute to tumor growth and/or metastatic potential in melanoma and that activation of AKT2 or AKT3 following PTEN loss may oppose the activity of AKT1 resulting in the different phenotypes we observed. Activating mutations in AKT1 and AKT3 have been detected in human melanoma and are associated with disease progression (Davies et al., 2008; Shi et al., 2014). Future studies will compare the effects of AKT2 and AKT3 in this context.

In this study, we observed significant differences in mammalian target of rapamycin complex (mTORC) pathway components between our PTEN deficient and myrAKT1 expressing melanomas suggesting an elevation of this signaling downstream of AKT activation. Hyperactive mTORC signaling is disproportionately observed in melanomas (73%; 78/107) compared to benign nevi (4%; 3/67) (Karbowniczek et al., 2008). Deletion of *Lkb1*, a known negative regulator of mTORC signaling, in *KRas* mutant mouse melanocytes results in the formation of highly metastatic melanomas in vivo (Liu et al., 2012). More recently, loss of *Lkb1* in the context of non-metastatic BRAF^{V600E}/INK4A-Arf^{Null} melanomas resulted in highly metastatic disease (Damsky et al., 2015). The pharmacological targeting of mTOR effectively blocks melanoma cell growth in vitro and in animal models (Dankort et al., 2009; Guba et al., 2002; Hidalgo and Rowinsky, 2000). Unfortunately, mTOR inhibitors have failed to demonstrate clinical efficacy against melanoma as mono-therapy and are currently being evaluated in combination with other therapies for this disease (Margolin et al., 2005). In line with increased mTORC signaling in melanoma metastasis, we found that total protein and phospho-protein levels of Rictor, an exclusive mTORC2 component, were significantly higher in myrAKT1-expressing melanomas than in PTEN-deficient melanomas (Figure 5; Figure S4). Combined inhibition of PI3K and mTOR has been shown to inhibit melanoma cell growth both in vitro and in vivo and interfere with angiogenesis (reviewed in Sznol et al., 2013). We observed that pharmacological inhibition of PI3K and mTOR also reduces melanoma cell migration. Taken together, our findings and those of others implicate increased mTORC signaling in promoting melanoma metastasis.

This model is ideally suited to further define the role of these proteins in melanoma metastasis, and future studies will focus on evaluating specific effectors downstream of AKT signaling in melanoma progression with the ultimate goal of identifying targets for therapies aimed at preventing or treating disseminated disease.

EXPERIMENTAL PROCEDURES

Vector Constructs
The retroviral vectors in this study are replication-competent avian leukosis virus, Bryan polymerase-containing vectors of envelope subgroup A (designated RCASBP(A) and abbreviated RCAS). RCAS-*Cre* and RCAS-myr*Akt1* have been described previously (Aoki et al., 1998; VanBrocklin et al., 2010).

Cell Culture
DF-1 cells were grown in DMEM-high glucose media supplemented with 10% FBS (Invitrogen), 50 ug/ml gentamicin (Invitrogen) and maintained at 39°C.

Migration Assays
Cell migration was evaluated for serum-starved cells with FBS as the chemoattractant using a modified boyden chamber assay (Cultrex 96 Well Cell Migration Assay, Trevigen) per the manufacturer's specifications.

Virus Propagation
Virus infection was initiated by calcium phosphate transfection of plasmid DNA into DF-1 cells. Viral spread was monitored by GFP positive control transfection and expression of the p27 viral capsid protein by western blot.

Western Blotting
Tumor lysates were suspended in RPPA buffer (Tibes et al., 2006) with protease and phosphatase inhibitors (Pierce Biotechnology), separated on a 4%–20% Tris-glycine polyacrylamide gel, and transferred to nitrocellulose for immunoblotting. Detailed experimental procedures and antibodies used are described in Supplemental Experimental Procedures.

Viral Infections In Vivo
Infected DF-1 cells from a confluent culture in a 10-cm dish were trypsinized, pelleted, resuspended in 50 μl PBS, and placed on ice. Newborn mice were injected subcutaneously behind the ear with 50 μl suspended myr*Akt1* cells and 50 μl suspended *Cre* cells.

Histology and Histochemical Staining
Mice were euthanized at their experimental endpoints set according to the guidelines of the University of Utah Institutional Animal Care and Use Committee. Mouse tissues were fixed in formalin overnight, dehydrated in 70% ethyl alcohol, and paraffin embedded. Sections were stained with H&E or left unstained for immunohistochemistry.

Immunohistochemistry
Tissue sections were hydrated, deparaffinized, and processed using the Biocare Medical HRP-Polymer system (Biocare Medical) according to the manufacturer's recommendations. Detailed procedures and antibodies used are described in Supplemental Experimental Procedures.

Reverse-Phase Protein Array
Frozen tumor tissue was embedded in optimum cutting temperature (OCT) compound. H&E-stained slides were reviewed by an experienced dermatopathologist (Alexander J. Lazar) to identify areas that contained >70% tumor cells. Regions with extensive necrosis, fibrosis, or hemorrhage within the tumor specimens were excluded. The H&E slides were used as a guide to macrodissect the OCT blocks and isolate tumor-enriched regions for further analysis. 10- to 20-μm tumor shears were generated by cryostat and were used for protein and total RNA extraction. Proteins were isolated from the tumor shears, and RPPA was performed as previously described (Davies et al., 2009; Tibes et al., 2006).

Mice and Genotyping
Dct::TVA;Cdkn2a^lox/lox^*;Braf*^CA^ mice (designated as *Pten*^WT^) and *Dct::TVA; Cdkn2a*^lox/lox^*;Braf*^CA^*; Pten*^lox/lox^ mice (referred to as *Pten*^lox/lox^) were generated via crossing previously existing genetically engineered mice. All mice were maintained on a mixed C57Bl/6 and FVB/N background by random interbreeding. DNA from tail biopsies was used to genotype for the *Dct::TVA* transgene, *Cdkn2a*^lox^, *Braf*^CA^, *Pten*^lox^ and wild-type alleles as described previously (Dankort et al., 2007; VanBrocklin et al., 2010; Zheng et al., 2008).

Statistical Analysis
Censored survival data were analyzed using a log-rank test of the Kaplan-Meier estimate of survival. Densitometry of the western blot was performed using ImageJ (Schneider et al., 2012), and the data are presented as mean ± SEM. Student's t test was used to compare migration between control and treated cells as well as protein expression levels between groups in the RPPA analysis. Protein-protein coefficients were determined by the Pearson correlation method, and the significance of the interactions was determined by the t statistic using R software. Unsupervised hierarchical clustering of mean-centered protein expression values was done using Cluster 2.1 and Treeview software.

Study Approval
All animal experimentation was performed in Association for Assessment and Accreditation of Laboratory Animal Care (AAALAC)-approved facilities at the University of Utah. All animal protocols were reviewed and approved prior to experimentation by the Institutional Animal Care and Use Committee at the University of Utah.

SUPPLEMENTAL INFORMATION

Supplemental information includes Supplemental Experimental Procedures, five figures, and two tables and can be found with this article online at http://dx.doi.org/10.1016/j.celrep.2015.09.057.

AUTHOR CONTRIBUTIONS

J.H.C. and J.P.R. contributed to the experimental design and performed the majority of the experiments. R.A.A., W.J.B., and D.A.K. performed immunohistochemistry and immunoblotting. G.C. and M.A.D. were responsible for the reverse-phase protein array experiments. A.H.G. provided pathological analysis. M.W.V., M.M., and S.L.H. were responsible for mouse model establishment, tumor induction, and characterization. J.H.C., M.M., and S.L.H. prepared the manuscript.

ACKNOWLEDGMENTS

REFERENCES

Aguirre, A.J., Bardeesy, N., Sinha, M., Lopez, L., Tuveson, D.A., Horner, J., Redston, M.S., and DePinho, R.A. (2003). Activated Kras and Ink4a/Arf

deficiency cooperate to produce metastatic pancreatic ductal adenocarcinoma. Genes Dev. *17*, 3112–3126.

Aoki, M., Batista, O., Bellacosa, A., Tsichlis, P., and Vogt, P.K. (1998). The akt kinase: molecular determinants of oncogenicity. Proc. Natl. Acad. Sci. USA *95*, 14950–14955.

Chalhoub, N., and Baker, S.J. (2009). PTEN and the PI3-kinase pathway in cancer. Annu. Rev. Pathol. *4*, 127–150.

Damsky, W., Micevic, G., Meeth, K., Muthusamy, V., Curley, D.P., Santhanakrishnan, M., Erdelyi, I., Platt, J.T., Huang, L., Theodosakis, N., et al. (2015). mTORC1 activation blocks BrafV600E-induced growth arrest but is insufficient for melanoma formation. Cancer Cell *27*, 41–56.

Dankort, D., Filenova, E., Collado, M., Serrano, M., Jones, K., and McMahon, M. (2007). A new mouse model to explore the initiation, progression, and therapy of BRAFV600E-induced lung tumors. Genes Dev. *21*, 379–384.

Dankort, D., Curley, D.P., Cartlidge, R.A., Nelson, B., Karnezis, A.N., Damsky, W.E., Jr., You, M.J., DePinho, R.A., McMahon, M., and Bosenberg, M. (2009). Braf(V600E) cooperates with Pten loss to induce metastatic melanoma. Nat. Genet. *41*, 544–552.

Davies, M.A., Stemke-Hale, K., Tellez, C., Calderone, T.L., Deng, W., Prieto, V.G., Lazar, A.J., Gershenwald, J.E., and Mills, G.B. (2008). A novel AKT3 mutation in melanoma tumours and cell lines. Br. J. Cancer *99*, 1265–1268.

Davies, M.A., Stemke-Hale, K., Lin, E., Tellez, C., Deng, W., Gopal, Y.N., Woodman, S.E., Calderone, T.C., Ju, Z., Lazar, A.J., et al. (2009). Integrated Molecular and Clinical Analysis of AKT Activation in Metastatic Melanoma. Clin. Cancer Res. *15*, 7538–7546.

Deuker, M.M., Marsh Durban, V., Phillips, W.A., and McMahon, M. (2015). PI3′-kinase inhibition forestalls the onset of MEK1/2 inhibitor resistance in BRAF-mutated melanoma. Cancer Discov. *5*, 143–153.

Dummler, B., Tschopp, O., Hynx, D., Yang, Z.Z., Dirnhofer, S., and Hemmings, B.A. (2006). Life with a single isoform of Akt: mice lacking Akt2 and Akt3 are viable but display impaired glucose homeostasis and growth deficiencies. Mol. Cell. Biol. *26*, 8042–8051.

Girotti, M.R., Saturno, G., Lorigan, P., and Marais, R. (2014). No longer an untreatable disease: how targeted and immunotherapies have changed the management of melanoma patients. Mol. Oncol. *8*, 1140–1158.

Gonzalez, E., and McGraw, T.E. (2009). The Akt kinases: isoform specificity in metabolism and cancer. Cell Cycle *8*, 2502–2508.

Guba, M., von Breitenbuch, P., Steinbauer, M., Koehl, G., Flegel, S., Hornung, M., Bruns, C.J., Zuelke, C., Farkas, S., Anthuber, M., et al. (2002). Rapamycin inhibits primary and metastatic tumor growth by antiangiogenesis: involvement of vascular endothelial growth factor. Nat. Med. *8*, 128–135.

Hidalgo, M., and Rowinsky, E.K. (2000). The rapamycin-sensitive signal transduction pathway as a target for cancer therapy. Oncogene *19*, 6680–6686.

Karbowniczek, M., Spittle, C.S., Morrison, T., Wu, H., and Henske, E.P. (2008). mTOR is activated in the majority of malignant melanomas. J. Invest. Dermatol. *128*, 980–987.

Linnerth-Petrik, N.M., Santry, L.A., Petrik, J.J., and Wootton, S.K. (2014). Opposing functions of Akt isoforms in lung tumor initiation and progression. PLoS ONE *9*, e94595.

Liotta, L.A., Espina, V., Mehta, A.I., Calvert, V., Rosenblatt, K., Geho, D., Munson, P.J., Young, L., Wulfkuhle, J., and Petricoin, E.F., 3rd. (2003). Protein microarrays: meeting analytical challenges for clinical applications. Cancer Cell *3*, 317–325.

Liu, W., Monahan, K.B., Pfefferle, A.D., Shimamura, T., Sorrentino, J., Chan, K.T., Roadcap, D.W., Ollila, D.W., Thomas, N.E., Castrillon, D.H., et al. (2012). LKB1/STK11 inactivation leads to expansion of a prometastatic tumor subpopulation in melanoma. Cancer Cell *21*, 751–764.

Madhunapantula, S.V., and Robertson, G.P. (2011). Therapeutic Implications of Targeting AKT Signaling in Melanoma. Enzyme Res. *2011*, 327923.

Majumder, P.K., Yeh, J.J., George, D.J., Febbo, P.G., Kum, J., Xue, Q., Bikoff, R., Ma, H., Kantoff, P.W., Golub, T.R., Loda, M., and Sellers, W.R. (2003). Prostate intraepithelial neoplasia induced by prostate restricted Akt activation: the MPAKT model. Proc. Natl. Acad. Sci. USA *100*, 7841–7846.

Margolin, K., Longmate, J., Baratta, T., Synold, T., Christensen, S., Weber, J., Gajewski, T., Quirt, I., and Doroshow, J.H. (2005). CCI-779 in metastatic melanoma: a phase II trial of the California Cancer Consortium. Cancer *104*, 1045–1048.

Maroulakou, I.G., Oemler, W., Naber, S.P., and Tsichlis, P.N. (2007). Akt1 ablation inhibits, whereas Akt2 ablation accelerates, the development of mammary adenocarcinomas in mouse mammary tumor virus (MMTV)-ErbB2/neu and MMTV-polyoma middle T transgenic mice. Cancer Res. *67*, 167–177.

Marsh Durban, V., Deuker, M.M., Bosenberg, M.W., Phillips, W., and McMahon, M. (2013). Differential AKT dependency displayed by mouse models of BRAFV600E-initiated melanoma. J. Clin. Invest. *123*, 5104–5118.

Nogueira, C., Kim, K.H., Sung, H., Paraiso, K.H., Dannenberg, J.H., Bosenberg, M., Chin, L., and Kim, M. (2010). Cooperative interactions of PTEN deficiency and RAS activation in melanoma metastasis. Oncogene *29*, 6222–6232.

Ohsie, S.J., Sarantopoulos, G.P., Cochran, A.J., and Binder, S.W. (2008). Immunohistochemical characteristics of melanoma. J. Cutan. Pathol. *35*, 433–444.

Peng, X.D., Xu, P.-Z., Chen, M.L., Hahn-Windgassen, A., Skeen, J., Jacobs, J., Sundararajan, D., Chen, W.S., Crawford, S.E., Coleman, K.G., and Hay, N. (2003). Dwarfism, impaired skin development, skeletal muscle atrophy, delayed bone development, and impeded adipogenesis in mice lacking Akt1 and Akt2. Genes Dev. *17*, 1352–1365.

Schneider, C.A., Rasband, W.S., and Eliceiri, K.W. (2012). NIH Image to ImageJ: 25 years of image analysis. Nat. Methods *9*, 671–675.

Shi, H., Hong, A., Kong, X., Koya, R.C., Song, C., Moriceau, G., Hugo, W., Yu, C.C., Ng, C., Chodon, T., et al. (2014). A novel AKT1 mutant amplifies an adaptive melanoma response to BRAF inhibition. Cancer Discov. *4*, 69–79.

Stahl, J.M., Sharma, A., Cheung, M., Zimmerman, M., Cheng, J.Q., Bosenberg, M.W., Kester, M., Sandirasegarane, L., and Robertson, G.P. (2004). Deregulated Akt3 activity promotes development of malignant melanoma. Cancer Res. *64*, 7002–7010.

Sznol, J.A., Jilaveanu, L.B., and Kluger, H.M. (2013). Studies of NVP-BEZ235 in melanoma. Curr. Cancer Drug Targets *13*, 165–174.

Tibes, R., Qiu, Y., Lu, Y., Hennessy, B., Andreeff, M., Mills, G.B., and Kornblau, S.M. (2006). Reverse phase protein array: validation of a novel proteomic technology and utility for analysis of primary leukemia specimens and hematopoietic stem cells. Mol. Cancer Ther. *5*, 2512–2521.

VanBrocklin, M.W., Robinson, J.P., Lastwika, K.J., Khoury, J.D., and Holmen, S.L. (2010). Targeted delivery of NRASQ61R and Cre-recombinase to postnatal melanocytes induces melanoma in Ink4a/Arflox/lox mice. Pigment Cell Melanoma Res. *23*, 531–541.

Wang, S., Gao, J., Lei, Q., Rozengurt, N., Pritchard, C., Jiao, J., Thomas, G.V., Li, G., Roy-Burman, P., Nelson, P.S., Liu, X., and Wu, H. (2003). Prostate-specific deletion of the murine Pten tumor suppressor gene leads to metastatic prostate cancer. Cancer Cell *4*, 209–221.

Yang, Z.-Z., Tschopp, O., Di-Poï, N., Bruder, E., Baudry, A., Dümmler, B., Wahli, W., and Hemmings, B.A. (2005). Dosage-dependent effects of Akt1/protein kinase Balpha (PKBalpha) and Akt3/PKBgamma on thymus, skin, and cardiovascular and nervous system development in mice. Mol. Cell. Biol. *25*, 10407–10418.

Zheng, H., Ying, H., Yan, H., Kimmelman, A.C., Hiller, D.J., Chen, A.J., Perry, S.R., Tonon, G., Chu, G.C., Ding, Z., et al. (2008). p53 and Pten control neural and glioma stem/progenitor cell renewal and differentiation. Nature *455*, 1129–1133.